U.S. DEPARTMENT OF ENERGY

DOE/SC-ARM/ TR-089

WACR Calibration Study

J Mead

March 2010

ARM

CLIMATE RESEARCH FACILITY

DISCLAIMER

DOE/SC-ARM/ TR-089

WACR Calibration Study

Submitted by

ProSensing Inc.
107 Sunderland Road
Amherst, MA 01002-1098, USA

March 2010

Work supported by the U.S. Department of Energy,
Office of Science, Office of Biological and Environmental Research

Contents

Figures

Tables

1.0 Radar Range Equation Error Analysis

1.1 Derivation of the Radar Range Equation for Cloud Radars

Following the development presented in section 5-14 of [1], the total scattering volume radar cross section, σ, can be expressed as:

$$\sigma = \sigma_v V_w = \frac{(4\pi)^3 R^4 P_r}{G_0^2 \lambda^2 P_t} \tag{1}$$

where P_r is the received power at the antenna terminals, P_t is the transmit power, G_o is the peak antenna gain, and *R* is the target range. The radar cross section is equal to the backscattering cross section per unit volume, σ_v, times the weighted volume, V_w, illuminated by the radar:

$$V_w = \frac{c\tau}{2l_r} \iint_{\theta,\phi} g(\theta,\phi)^2 d\phi d\theta$$

where $g(\theta,\phi)$ is the normalized antenna gain pattern in azimuth (θ) and elevation (ϕ) and $\frac{c\tau}{2l_r}$ is the effective length of the pulse volume in meters, corrected for finite receiver bandwidth effects through the loss factor, l_r [2]. Assuming a symmetric, Gaussian antenna beam pattern, V_w can be approximated by [3]

$$V_w = \pi \cdot \frac{c\tau R^2 \theta_{3dB}^2}{l_r 16 \ln(2)} \tag{2}$$

where θ_{3dB} is the antenna's one-way half power beam width. Substituting (2) into (1) yields

$$\sigma_v = \frac{1024 \ln(2) \pi^2 l_r R^2 P_r}{c\tau G_0^2 \lambda^2 \theta_{3dB}^2 P_t} \qquad \frac{m^2}{m^3} \tag{3}$$

The radar range equation for a point, or corner, reflector is given by

$$\sigma_c = \frac{(4\pi)^3 R_c^4 P_{rc}}{G_0^2 \lambda^2 P_t} \tag{4}$$

where the subscript "c" refers to a corner reflector.

Equation 4 can be rearranged as follows:

$$\frac{G_0^2 \lambda^2 P_t}{(4\pi)^3} = \frac{R_c^4 P_{rc}}{\sigma_c} \tag{5}$$

Equation (1) can also be rearranged to pull out the same constants:

$$\frac{G_0^2 \lambda^2 P_t}{(4\pi)^3} = \frac{R^4 P_r}{\sigma_v V_w} \tag{6}$$

Equating (5) and (6) and substituting (2) for V_w yields the following expression for σ_v:

$$\sigma_v = \frac{16 \ln(2) l_r R^2 \sigma_c}{\pi c \tau R_c^4 \theta_{3dB}^2} \left(\frac{P_r}{P_{rc}} \right) \tag{7}$$

Note that both P_r and P_{rc} are scaled by the receiver gain and the transfer function of the digital receiver.

From section 5.11.3 in [1], σ_v is related to the cloud reflectivity factor, Z in $\frac{mm^6}{m^3}$, by

$$\sigma_v = 10^{-18} \frac{\pi^5}{\lambda^4} |K|^2 Z \tag{8}$$

where *K* is a function of the complex index of refraction, *n*:

$$K = \frac{n^2 - 1}{n^2 + 2}$$

For liquid water at 95 GHz, $0^\circ C$, $|K| = 0.84$.

Combining (7) and (8) gives Z as:

$$Z = \frac{16 \ln(2) l_r \lambda^4 \sigma_c}{10^{-18} c \tau \pi^6 |K|^2 \theta_{3dB}^2} \frac{R^2}{R_c^4} \frac{P_R}{P_{RC}} \qquad \frac{m^2}{m^3} \tag{9}$$

This derivation assumes no appreciable atmospheric attenuation between the radar and the corner reflector or between the radar and the cloud. These loss factors can be included as total two-way path attenuation factors between the radar and scattering volume, l_a, $1.0 < l_a \leq \infty$ and between the radar and corner reflector, l_{ac}, $1.0 < l_{ac} \leq \infty$ with 1.0 being no attenuation:

$$Z = \frac{16 \ln(2) l_r \lambda^4 \sigma_c}{10^{-18} c \tau \pi^6 |K|^2 \theta_{3dB}^2} \frac{R^2}{R_c^4} \frac{P_R l_a}{P_{RC} l_{ac}} \qquad \frac{m^2}{m^3} \tag{10}$$

1.2 Error Analysis

There are a number of sources of error in computing reflectivity. Equation (10) can be re-expressed to explicitly highlight parameters that have uncertainty:

$$Z = \frac{\Gamma \sigma_c}{V_w 10^{-18} \pi^5 |K|^2} \frac{R^4}{R_c^4} \frac{P_R l_a}{P_{RC} l_{ac}} \qquad \frac{m^2}{m^3} \tag{11}$$

where all of the fixed constants are lumped into a single variable, $\Gamma = \frac{\lambda^4}{10^{-18} \pi^5}$.

Re-expressing (11) in dBZ gives:

$$dBZ = 10\log Z = 10\log\Gamma + 10\log\sigma_c + 40\log R + 10\log P_r + 10\log l_a - 40\log R_c - 10\log P_c - 10\log l_{ac} \tag{12}$$

Taking the derivative of (12) with respect to individual parameters yields the sensitivity of dBZ to changes in those parameters:

$$\frac{d(dBZ)}{d(10\log\sigma_c)} = 1$$

$$\frac{d(dBZ)}{d(10\log R)} = 4$$

$$\frac{d(dBZ)}{d(10\log P_R)} = 1$$

$$\frac{d(dBZ)}{d(10\log l_a)} = 1$$

$$\frac{d(dBZ)}{d(10\log V_w)} = -1$$

$$\frac{d(dBZ)}{d(10\log|K|)} = -2$$

$$\frac{d(dBZ)}{d(10\log R_c)} = -4$$

$$\frac{d(dBZ)}{d(10\log P_c)} = -1$$

$$\frac{d(dBZ)}{d(10\log l_{ac})} = -1$$

Thus, a +x dB error in the corner reflector radar cross section will result in a +x dB error in dBZ, while a +y dB error in estimating the index of refraction factor, $|K|$, will map into a -2y dB error in dBZ. Note that not all of these parameters vary independently. For example, the illuminated volume increases as the square of the target range and inversely with antenna gain.

The error sources in measured reflectivity are summarized below:

- Errors in the corner reflector radar cross-section due to manufacturing, signal-to-clutter ratio, and switched-in receiver attenuation during calibration
- Errors in estimating the volume integral, V_w
- Errors associated with the scattering volume range and corner reflector range factors
- Uncertainty in the index of refraction of water due to temperature variation, causing errors in the assigned value of $|K|$.
- Errors associated with measuring the scattering volume and corner reflector power
- Propagation losses between the radar and calibration target and between the radar and cloud, including loss due to water deposition on the antenna.

Between calibrations, variations in receiver gain and transmit power will cause additional errors in the reported reflectivity.

The various error sources are considered separately below.

1.3 Corner Reflector Radar Cross-Section

The radar cross-section of trihedral corner reflectors that are large compared to the radar wavelength is accurately modeled by the following formula [1, Table 10.1]:

$$\sigma_c = \frac{\pi l^4}{3\lambda^2}$$

where *l* is the length of the front-face edge of the trihedral. For example, the corner reflector currently in use with WACR SGP has a front-face length of 6.4 inches, yielding a radar cross-section of 24.8 dB m^2.

1.3.1 Reflector Plate Angular Errors

Manufacturing errors will result in angular errors in the alignment of the metallic plates forming the trihedral. A formula relating angular errors to errors in radar cross section is given in [4]:

$$\frac{\sigma}{\sigma_{ideal}} = 10\log\left(\frac{\sin q}{q}\right)^4 dB$$

with $q = \frac{2.54\delta_{\max} D}{\lambda}$ where $\delta_{\max}$ in radians is the maximum angular deviation from 90 degrees among the plates and $D = l/\sqrt{2}$ is the length of the inside edge of the reflector.

Figure 1 plots the radar cross-section error as a function of the maximum angular error of the plates for the WACR corner reflector currently in use at SGP. This shows that the radar cross-section error is small for angular errors less than 0.1 degrees. Using modern manufacturing techniques, it is very likely that the RCS error due to plate misalignment is less than 0.1 dB and therefore represents a negligible source of measurement error.

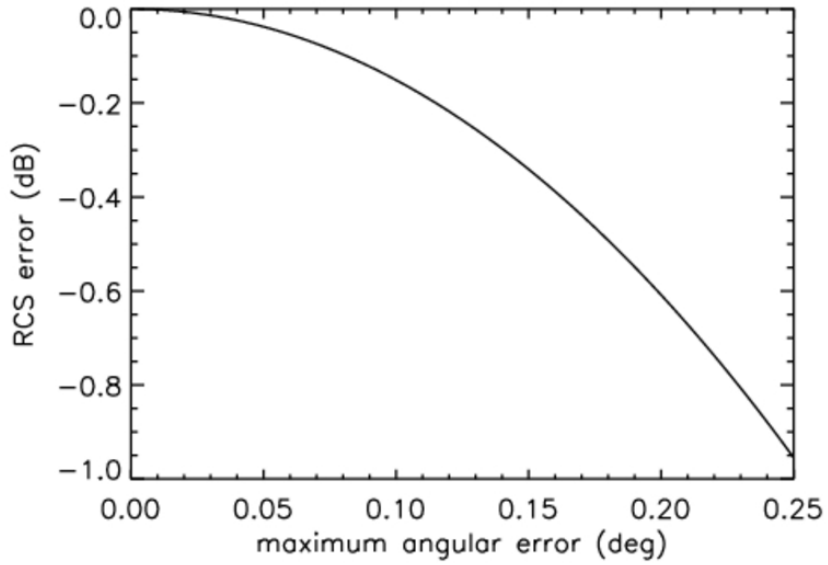

Figure 1. Corner reflector radar cross-section error as a function of maximum plate alignment error for a D=6.4 inch trihedral reflector at 95.04 GHz.

1.3.2 Reflector Alignment Error

Trihedral corner reflectors maintain a nearly constant radar cross-section over a range of angles. Data presented by [5] show that the radar cross-section of an electrically large reflector varied by only 1 dB over a range of +/-10 degrees. Visual inspection of the WACR SGP corner reflector indicates that the reflector face is aligned to within about +/-2 degrees, indicating that error due to reflector alignment is negligible.

1.3.3 Reflector Signal-to-Clutter Ratio

Reflections from the mast supporting the corner reflector can bias the corner reflector radar cross-section to a larger or smaller value, depending on the relative phase of the reflections. The maximum enhancement in RCS occurs when the reflections are in-phase and the greatest reduction in RCS when the reflections are out of phase. The maximum error, computed as a function of signal-to-clutter ratio [1, eq. 10.18] is plotted in Figure 2. The SCR for the WACR SGP reflector was measured to be approximately 30 dB, resulting in a maximum error of +/- 0.28 dB.

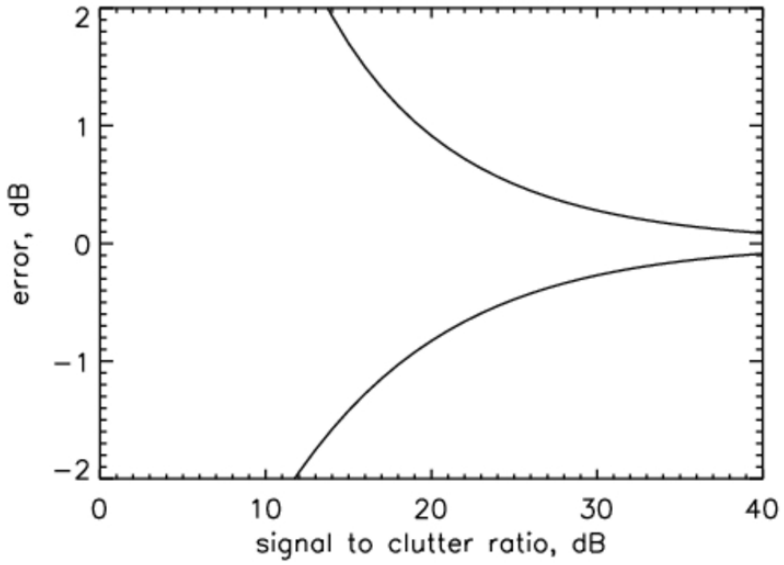

Figure 2. RCS error as a function of SCR. The lines show the maximum possible positive and negative error.

1.4 Volume Integral Estimation

The approximation of the pulse volume assumes a Gaussian beam pattern in the cross-range direction. Gaussian beam approximations are typically very good for high gain antennas. To confirm this, the antenna pattern of the WACR SGP system was measured by viewing the corner reflector at the SGP site and scanning in azimuth and elevation. These scans showed excellent agreement to a Gaussian approximation, down to the -20 dB level, as seen in Figure 3.

The shape of the pulse at the output of the digital receiver is plotted in Figure 4. This shape is very close to the expected response of a square pulse passed through the digital filter[1], which is close to a matched filter for a 300 ns pulse [6].

[1] Digital filter weights: 1132, 4095, 7059, 17x8191, 7059, 4095, and 1132.

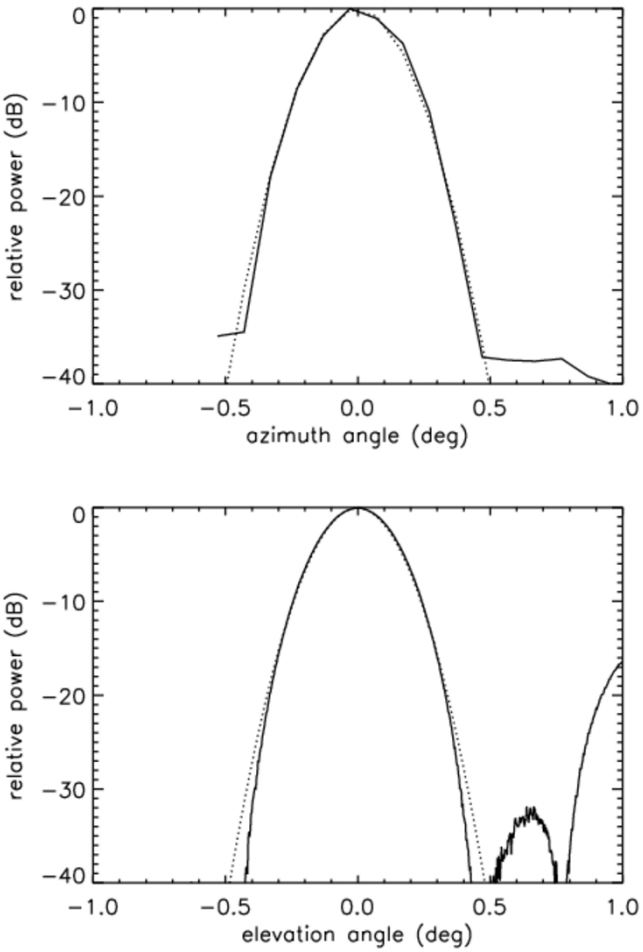

Figure 3. Azimuth (top) and elevation (bottom) two-way patterns of WACR SGP antenna with Gaussian fit shown as dotted line. The sidelobe in the elevation pattern at 1 degree is due to ground scattering from the main beam.

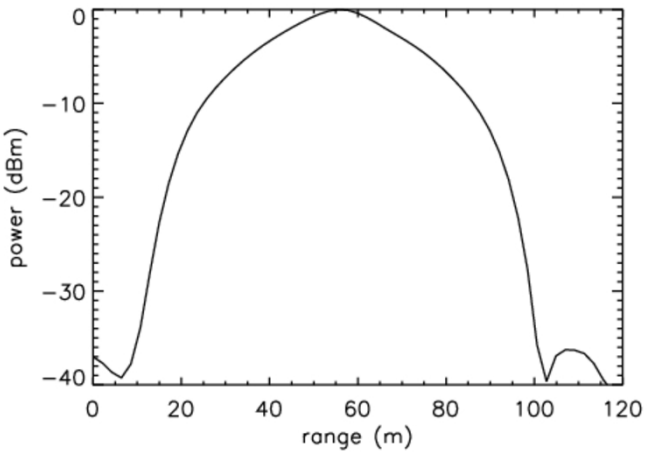

Figure 4. Pulse response versus range as measured at the peak of the corner reflector return.

The pulse volume was evaluated numerically at the corner reflector range and compared to the approximate value given by (2), as shown in Table 1. This analysis confirms that the pulse volume is accurately characterized by (2), and that the errors associated with assuming a constant range are negligible, even at a comparatively short range of 490 m.

Table 1. Radar pulse volume at 490 meters range to center of pulse volume, evaluated numerically and approximated using (2).

	Pulse volume assuming range is constant over the distance to the center of the range gate	**Pulse Vvlume, letting range equal true range to incremental volume**	**Approximation error, fixed vs. varying range**
Numerical integral	200. 5 m^3	202.5 m^3	.04 dB
Probert-Jones approximation	197.5 m^3	199.8 m^3	.05 dB
Approximation error, Numerical vs. Probert-Jones	.07 dB	.06 dB	

1.4.1 Temperature Dependence of the Index of Refraction of Water

The scattering cross section of small droplets is dependent on the value *K,* which is a function of the droplet index of refraction, *n* [1, eq. 5.73]:

$$K = \frac{n^2 - 1}{n^2 + 2}$$

The index of refraction of water is a function of frequency and temperature [1, Section E-2, pg. 2020]. This formulation was used to compute $|K|$ 95.0 GHz as a function of temperature (Figure 5), which shows a variation of 0.5 dB at 95.0 GHz over the temperature range 0–40 degrees C. Since reflectivity is dependent on $|K|^2$, uncompensated temperature variations map into a 1.0 dB reflectivity error at 95 GHz. The convention among radar meteorologists is to use a fixed value of $|K|$, since $|K|$ is not strongly temperature-dependent at conventional weather radar frequencies. It may also be sufficient to assume a constant value of $|K|$ at 95 GHz, provided an assumed value is agreed upon when making comparisons between different radar systems. As an example, CloudSat uses a value of $|K|^2 = .75$, or $|K| = .866$, which corresponds to a temperature of 8 degrees C. WACR uses $|K| = .84$.

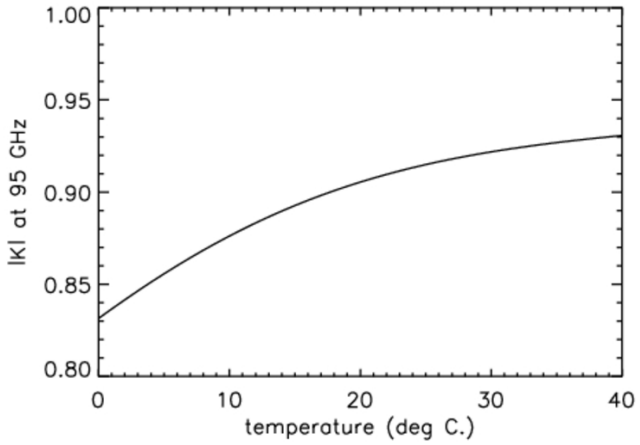

Figure 5. Temperature dependence of $|K|$ at 95 GHz.

1.4.2 Power Measurement Errors

The following error mechanisms can potentially contribute to power measurement errors:

1. Errors in the zeroth moment estimator that extracts signal power from the measured Doppler spectrum.
2. Errors in the transfer function used to map measured power into calibrated power. This is a problem that has been identified with MMCR.

1.4.2.1 Zeroth Spectral Moment Estimator

Both WACR and MMCR use moment estimators to extract the zeroth, first, and second moments of the Doppler spectrum. At low signal-to-noise ratio, the zeroth moment, corresponding to P_r in the range equation, can be biased either upward or downward, depending on the signal's spectral width relative to spectral resolution. Figure 6 plots zeroth-moment bias for WACR's standard operating mode as a function of the spectral peak signal-to-noise ratio for three cases: 0.2, 0.6, and 2.0 m/s spectral width.

To explain this behavior, consider the following conditions. If the signal spectrum is below the noise, then the moment estimator will overestimate signal power, since it treats noise peaks as signal even if no signal is present. If the spectrum is broad (relative to the spectral resolution) and slightly above the noise floor, then the moment estimator will underestimate signal power. This is because there is significant power in the signal spectrum that falls below the noise floor and is therefore ignored when computing the zeroth moment. If the spectrum is narrow, then the estimator works well at low signal-to- noise ratio, since the signal power is concentrated in a few spectral bins and is neither biased high by the first effect or biased low by the second effect.

The standard deviation of the zeroth-moment estimate is plotted as a function of the spectral peak signal-to-noise ratio in Figure 7 for three different spectral widths. As expected, the standard deviation is seen to be large for low signal-to-noise ratios. However, the standard deviation is not strongly dependent on spectral width.

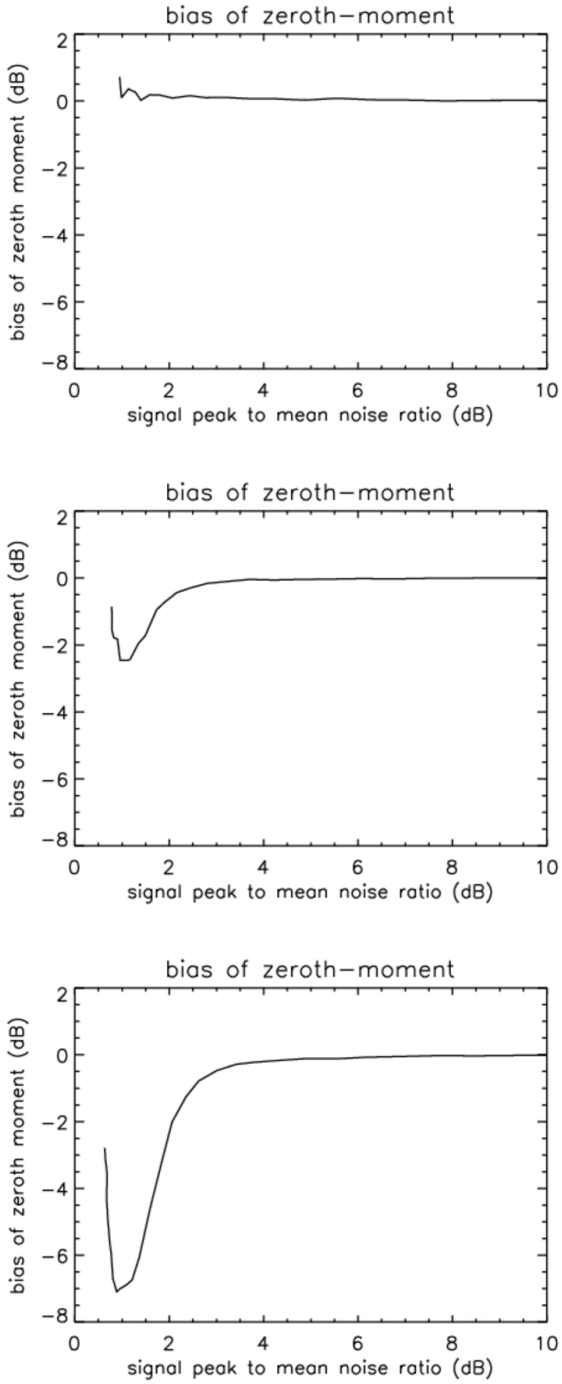

Figure 6. Simulated bias deviation of the zeroth spectral moment (P_r) as a function of the peak signal-to-mean-noise floor level for three spectral widths: 0.2 m/s (top), 0.6 m/s (middle), and 2.0 m/s (bottom); 10 kHz PRF; 256 point FFT; 2; 160 spectra averaged.

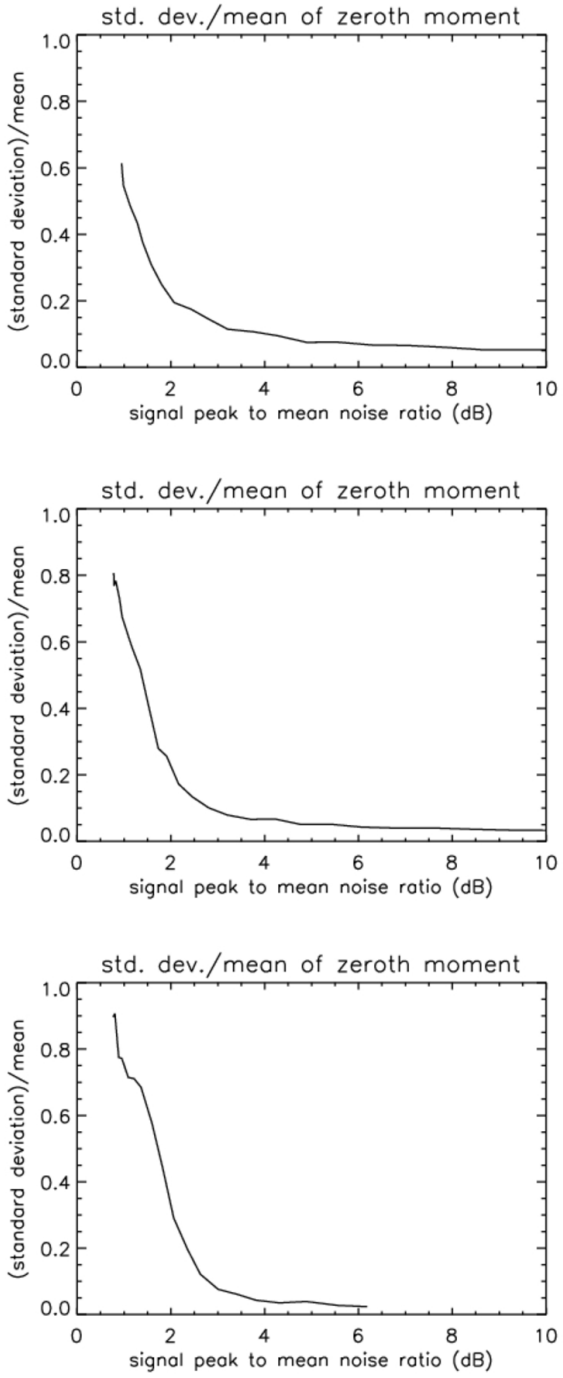

Figure 7. Simulated standard deviation relative to mean of the zeroth spectral moment (P_r) as a function of the peak signal-to-mean-noise floor level for three spectral widths: 0.2 m/s (top), 0.6 m/s (middle), and 2.0 m/s (bottom); 10 kHz PRF; 256 point FFT; 2; 160 spectra averaged.

1.4.3 Propagation Losses

WACR reflectivity is not compensated for propagation losses. Propagation losses at W-band arise from water vapor absorption and extinction due to hydrometeors.

1.4.3.1 Attenuation Due to Atmospheric Water Vapor

The total atmospheric loss factor from the ground through the top of the atmosphere is given by [Waters, 1976]:

$$\tau_0(dB) = 0.17 + .06\rho_0(g/m^3) \text{ at 90 GHz}$$

The range of zenith attenuation at W-band is .17 dB to 1.5 dB. Actual data plotted in [1, Fig. 5.8] show measured zenith attenuation at W-band as high as 2.0 dB. Most of this attenuation will occur in the boundary layer, where water vapor is concentrated. Thus, high clouds could experience as much as 3.0–4.0 dB two-way loss due to water vapor at W-band.

1.4.3.2 Attenuation Due to Hydrometeors

The extinction coefficient due to small liquid water droplet (Rayleigh approximation) is given by

$$\kappa_1 = .434\frac{6\pi}{\lambda_0}\text{Im}(-K) \quad \text{dB/km/g/m}^3.$$

For a wet cloud (1 g/m^3), κ_1 ranges from 3 to 5 dB/km at W-band (3 dB at 40°C; 5 dB at 0°C). The two-way loss will be double this amount, leading to significant errors in dBZ if uncorrected.

Loss in ice or snow is negligible at W-band.

1.4.3.3 Antenna/Radome Losses

Signal loss due to absorption and scattering from sheeting water on a radome can be significant. Lab measurements carried out at ProSensing at W-band showed that a low to moderate density of small droplets had minimal effect (less than 0.5 dB). However, when the droplet density becomes large with some regions of sheeting, the one-way loss was found to be 2–3 dB (4–6 dB two-way loss).

1.5 Errors Due to System Drift After Corner Reflector Calibration

1.5.1 Transmit Power and Receiver Gain Drift

WACR transmit power and receiver gain are monitored by the software, but the reported dBZ values are not adjusted for changes in these quantities. A sampling of variations in receiver gain and transmit power between 2005 and 2008 for WACR SGP and WACR AMF is summarized in Table 2 and Table 3. These data were taken when the radar was operating normally (data do not include periods of hardware failure).

Table 2. WACR SGP receiver gain and transmit power stability.

Date	Receiver Gain (dB)	Peak Transmit Power (W)
11/30/2005	39.1	1429
12/20/2005	39.4	1345
5/11/2006	39.5	1598
10/10/2006	39.0	1530
10/16/2006	39.4	1546
7/19/2007	38.9	1467
3/1/2008	39.8	1595
05/25/2008	39.7	1599
Mean standard deviation max deviation	39.4 dB .33 dB .5 dB	1513 W 93 W 168 W (.5 dB)

Table 3. WACR AMF receiver gain and transmit power stability.

Date	Receiver Gain (dB)	Peak Transmit Power (W)
2/1/2006	38.0	1344
2/20/2006	38.1	1382
4/25/2006	37.5	1363
12/27/2006	37.8	1364
2/26/2007	38.0	1315
3/13/2008	37.4	1317
Mean standard deviation max deviation	37.8 dB .29 dB .4 dB	1348 W 27 W 34 W (.1 dB)

1.6 Errors Specific to WACR AMF

The WACR AMF system had no provision for viewing a corner reflector. Therefore, its calibration coefficient was based on a computed value, much like MMCR.

1.7 Summary of Error Sources

Table 4 summarizes the various calibration error sources considered in this report. This table indicates that total calibration error should be small (< 3 dB) for targets above 10 dB SNR, under clear-air conditions with low humidity.

Variations in transmit power and receiver gain are small and are tracked by the data system. These data are not currently being used to correct the reported dBZ values.

Calibration error will rise dramatically when viewing clouds through liquid layers. Calibration error increases approximately 1 dB for each 0.1 g/m^3 per kilometer of cloud thickness in the propagation path between the radar and the layer under observation. (The addition of a radiometer mode could help correct for this loss).

Reflectivity bias at low SNR occurs due to errors in the moment estimator. This error is particularly pronounced when the cloud spectral width is large compared to the Doppler spectral resolution. The errors show up as both a bias and an increase in the standard deviation of the error, with the bias being largest at a ratio of 2.5 dB spectral peak power to mean spectral noise power ratio.

Table 4. Summary of calibration error sources in WACR.

Error Source	Error in reported WACR reflectivity
Corner reflector RCS	< 0.5 dB
Transmit power fluctuations	< .5 dB max deviation (unless EIKA near end of lifetime and excluding transmitter failure)
Receiver gain fluctuations	< 0.5 dB max deviation (excluding receiver failure)
Scattering volume/range errors	< .15 dB
Receiver power measurement	Up to 7 dB at low SNR due to errors in moment estimation (see Figure 6)
Index of refraction of water	+/- 0.5 dB over temperature
Propagation effects (two-way loss)	Water vapor: up to 3 dB error when viewing clouds above BL; reduced error for clouds in BL Liquid water: 8–10 dB/km for 1g/m^3 liquid cloud Water on radome: up to 6 dB for sheeting water

1.7.1 References

1. Ulaby, FT, RK Moore, and K Fung. 1986. *Microwave Remote Sensing, Active and Passive, Volume I and II.* Artech House, Norwood, MA.

2. Doviak, RJ and DS Zrnic. 1993. *Doppler Radar and Weather Observations, 2nd Edition***.** Academic Press, San Diego, equation 4.15.

3. Probert-Jones, JR. 1962. "The radar equation in meteorology." *Journal of the Royal Meteorological Society* 88: 485-495.

4. Craeye, C, P Sobieski, E Robin, and A Guissard. 1997. "Angular errors in trihedrals used for radar calibrations." *International Journal of Remote Sensing* 18(12): 2683-2689.

5. Robertson, SD. 1947. "Targets for microwave radar navigation." *Bell System Technical Journal* 26: 852-869.

6. WACR SGP Operations Manual, June, 2005, Table 5.

7. Waters, JW. 1976. "Absorption and emission of microwave radiation by atmospheric gases." In *Methods of Experimental Physics*. M.L. Meeks, ed., 12, Part B, Radio Astronomy, Academic Press, Section 2.3.

www.arm.gov